

## Supplementary Materials for **Tectonic control of Yarlung Tsangpo Gorge revealed by a buried canyon in Southern Tibet**

Ping Wang, Dirk Scherler,\* Jing Liu-Zeng, Jürgen Mey,  
Jean-Philippe Avouac, Yunda Zhang, Dingguo Shi

\*Corresponding author. E-mail: scherler@caltech.edu

Published 21 November 2014, *Science* **346**, 978 (2014)  
DOI: 10.1126/science.1259041

### This PDF file includes:

Materials and Methods  
Supplementary Text  
Figs. S1 to S7  
Tables S1 to S3  
References

## **Materials and Methods**

### Yarlung Tsangpo shallow drilling

To investigate the nature and amount of trapped sediments along the Yarlung Tsangpo, a series of exploratory shallow drillings were undertaken along the trunk river on point bars, riverbanks, and high terraces. The drillings (Figure S1) were located on modern riverbanks, no more than 20 m above the current river level. Each site consisted of an array of drillings, tens of meters apart, which reached bedrock (Figure S2, S3) and from which the deepest drill core was selected for analysis. However, there is no guarantee that the deepest position has been reached and thus the measured depth to bedrock should be considered a minimum estimate of the true depth to bedrock. Grain size data for cores #3-5, which were accessible for scientific analysis, is based on estimation during on-site visual inspection of the drill cores (Figure S1). A stratigraphic division of the deposits in the drill core from site #3 is provided in Table S1.

### Depth to bedrock

Ground-truth point measurements of the depth to bedrock are given by the drill cores. We obtained a first estimate of the depth to bedrock between the core locations by projecting hillslopes into the subsurface at a constant angle of 30°, which corresponds to the average hillslope angle within the Yarlung Tsangpo Valley (Fig. 2B). Reasonable agreement with the drill core data motivated us to reconstruct the bedrock beneath the valley fill using an artificial neural network (ANN), based on the approach in ref. 31. We used a 2-layer ANN with 10 hidden nodes and estimated the depth to bedrock at each valley-fill pixel in a 180-m resolution digital elevation model (DEM) based on the distance to hillslopes within 2 different sectors. The ANN was initially trained on hillslopes above the valley fill and within a maximum distance of 5 km from the valley floor. The valley-fill mask was based on manual digitization using Google Earth and local slope angles. We extended our depth to bedrock estimation not farther upstream than core location #1, where the depth to bedrock is 70 m, and where the channel width equals the valley floor width.

### Cosmogenic nuclide sample preparation

Three samples, each of 2-3 kg sand, were collected from the drill core at a depth of 561-564 m, directly overlying a 2-m thick cobble layer that rests on bedrock. After washing and cleaning, the sand was sieved and the grain size fraction of 250-500 µm was used for further analysis. Subsequent procedures for purifying quartz separates are based on the methods described in ref. 32: First, the samples were soaked overnight in HCl/H<sub>2</sub>O<sub>2</sub> to remove carbonate, iron oxide coating and organic matter. The samples were then leached for at least 9 hours at a constant temperature of 80°C in diluted HF/HNO<sub>3</sub> solution in an ultrasonic bath to remove meteoric <sup>10</sup>Be and other minerals except for quartz. The leaching and subsequent drying was repeated five times. Residual impurities were removed by heavy-liquid and hand separation under the microscope and the samples were once more treated with diluted HF/HNO<sub>3</sub> solution and dried. Aliquots of two grams were taken from each sample, dissolved in concentrated HF/HNO<sub>3</sub> and analysed by Inductively Coupled Plasma Optical Emission Spectrometer (ICP-OES) measurements for <sup>27</sup>Al and other elements to assure purity. The remaining quartz was spiked with 0.25

mg of  $^{9}\text{Be}$  in a weak  $\text{HNO}_3$  carrier solution, and then heated and dissolved. Fluorides were removed by fuming with  $\text{HNO}_3/\text{HClO}_4$ . The resulting samples were dissolved in pure water and  $\text{HClO}_4$ , heated and dried two times, then rinsed out with  $\text{HCl}$ .  $\text{Al}^{3+}$  and  $\text{Be}^{2+}$  were isolated using ion exchange resin, and neutralized by ammonia water to yield  $\text{Al(OH)}_3$  and  $\text{Be(OH)}_2$ . The oxides were separated gravitationally, transferred to quartz crucibles, and dried. The samples were baked at  $750^\circ\text{C}$ , yielding powder of  $\text{Al}_2\text{O}_3$  and  $\text{BeO}$ . These samples were sent to the Cosmogenic Nuclide Laboratory of the European Center for Earth Sciences, Environment Research and Education (CEREGE) in France for target preparation and measurement of the  $^{10}\text{Be}/^{9}\text{Be}$  and  $^{26}\text{Al}/^{27}\text{Al}$  ratios (Table S2). The ratios were measured relative to the standard NIST4325 with a nominal  $^{10}\text{Be}/^{9}\text{Be}$  ratio of  $2.79 \times 10^{-11}$ , and SM-Al-11, with a nominal  $^{26}\text{Al}/^{27}\text{Al}$  ratio of  $7.401 \times 10^{-12}$ . Our process blank  $^{10}\text{Be}/^{9}\text{Be}$  ratio was  $2.7 \times 10^{-15}$  and the corresponding  $^{10}\text{Be}$  atoms were subtracted from the reported sample results. Analytical uncertainties as well as uncertainties in the carrier and blanks were propagated using standard error-propagation methods. The lab-specific standard uncertainty (standard deviation) of the ICP-OES measurement of Al, regularly calibrated using standard blanks, is 5%.

### Burial dating

In steadily eroding landscapes, rocks are moving towards the Earth's surface with time and accumulate both  $^{10}\text{Be}$  and  $^{26}\text{Al}$  at rate that depends on the depth below the surface, the density of the overlying material and the geographic position (33). For  $^{10}\text{Be}$  and  $^{26}\text{Al}$ , three main production mechanisms exist. At shallow depths, most of the production occurs by spallation, but the production rate decreases rather rapidly with depth. At greater depths (>several meters in most materials), the production of cosmogenic nuclides is dominated by negative and fast muons, with the production rates being much lower compared to spallation and decreasing with depth at a slower rate (34). Because transport on hillslopes and in rivers is usually fast compared to exhumation on hillslopes, the cosmogenic nuclide concentration of river sediment can be used to calculate catchment-averaged hillslope erosion rates (35). When river sediment is deposited and gets successively buried to greater depths, at first, cosmogenic nuclides will continue to build up at a rate that depends, similar to hillslope erosion, on the rate of burial and the density of the deposited sediment. At sufficiently large depths, production rates are negligible and as time proceeds, the  $^{10}\text{Be}$  and  $^{26}\text{Al}$  atoms in the sediment will decay at a rate defined by the radioactive half-life (36). The half-life of  $^{10}\text{Be}$  is  $1.387 \pm 0.012$  (37,38) while the half-life of  $^{26}\text{Al}$  is  $0.705 \pm 0.024$  Ma (39). Burial dating with  $^{10}\text{Be}$  and  $^{26}\text{Al}$ , relies on the fact that both, the production rates and the half-lives of  $^{10}\text{Be}$  and  $^{26}\text{Al}$  are known, so that deviations from the steady exposure  $^{26}\text{Al}/^{10}\text{Be}$  ratio of ~7:1 can be converted to a burial age.

We modelled the concentration of cosmogenic nuclides,  $N$  (atoms  $\text{g}^{-1}$ ), as a function of depth below the surface,  $z$ , which we made to be a function of time since deposition,  $t$ , according to (40):

$$N(z,t) = N_{inh} e^{-\lambda t} + \int_0^t [P_n(z(t')) + P_\mu(z(t'))] e^{-\lambda t'} dt' \quad (\text{S1})$$

where,  $N_{inh}$  is the inherited concentration,  $\lambda$  is the decay constant, and  $P_n$  and  $P_\mu$  are the depth-dependent production rates by neutrons and muons, respectively. The decline of cosmogenic nuclide production by neutrons with depth depends on the material

density,  $\rho$ , and follows an exponential decline with an attenuation length scale,  $\Lambda$ , of  $\sim 160$  g cm $^{-2}$  (34)

$$P(z) = P_0 e^{-z\rho/\Lambda} \quad (\text{S2}).$$

The depth-dependency of cosmogenic nuclide production by muons is more complicated and we use the formulation of ref. (41,42), as adopted by ref. (43), and provided in the numerical functions of the CRONUS Earth online calculator ([http://hess.ess.washington.edu/math/al\\_be\\_v22/functionlist.html](http://hess.ess.washington.edu/math/al_be_v22/functionlist.html)). Different analytical approximations exist to capture the depth-dependency of cosmogenic nuclide production by muons with a series of exponentials. We use the formulation of ref. (40) to account for the inherited component in equation S1 ( $N_{inh}$ ), which corresponds to the cosmogenic nuclides that were produced during hillslope exhumation. At steady state, the concentration of cosmogenic nuclides at the Earth's surface is a function of the erosion rate,  $\varepsilon$  (44):

$$N(\varepsilon) = \sum_{i=0}^3 \frac{P_i(0)}{\lambda + \frac{\varepsilon\rho}{\Lambda_i}} \quad (\text{S3}).$$

where  $P_i(0)$  are the surface production rates due to neutrons ( $i=0$ ), negative muons ( $i=1,2$ ) and fast muons ( $i=3$ ), and  $\Lambda_i$  are the effective attenuation length scales ( $\Lambda_0 = 160$  g cm $^{-2}$ ,  $\Lambda_1 = 738.6$  g cm $^{-2}$ ,  $\Lambda_2 = 2688$  g cm $^{-2}$ , and  $\Lambda_3 = 4360$  g cm $^{-2}$ ). Using the MATLAB® functions of the CRONUS-Earth online calculator (v. 2.2) (43), we calculated site specific surface production rates due to spallation based on a time-dependent version of the scaling model by ref. (33) and ref. (45), which is denoted 'Lm' in the CRONUS-Earth online calculator (43). Muogenic production rates are compensated for local air pressure following ref. (45).

For calculating the cosmogenic nuclide concentrations acquired during hillslope exhumation using eq. S3, we computed average surface production rates for areas that are upstream of the sampling site. As these areas are very large and it may well be that different parts of this area did not contribute to our sample at all, we tested the influence of different upstream areas on average production rates. For upstream areas of  $\sim 300$ -1900 km $^2$  that successively entail larger areas upstream from the sampling point (drill core #3), average surface production rates vary between 10.3 and 12.3 atoms (g qz) $^{-1}$  yr $^{-1}$ , and are thus relatively insensitive to the exact extent of the contributing areas. However, our uncertainty in the extent of the contributing area means that we cannot use the paleo-erosion rates to estimate sediment fluxes from upstream. For the pre-burial production, we assume a rock density of 2.7 g cm $^{-3}$ .

One requirement for burial dating is that the pre-burial  $^{26}\text{Al}/^{10}\text{Be}$  ratio is known. For samples that have been continuously exposed to cosmic radiation this ratio reflects the differences in the production rates of  $^{26}\text{Al}$  and  $^{10}\text{Be}$ . However, if the grains in our samples have experienced burial and exhumation prior to deposition in the valley fill, the  $^{26}\text{Al}/^{10}\text{Be}$  ratio may be lower than for continuous exposure. This would result in an overestimated burial age. However, we don't think that this effect is particularly important for the following reasons. First, significant shifts in the  $^{26}\text{Al}/^{10}\text{Be}$  ratio requires rather long ( $>10^5$  yrs) burial at sufficiently great depths ( $>\sim 10$  m). Although temporary storage may be quite common, for longer and deeper burial histories, it is less likely that the sediment is remobilized. In other words, the number of grains with low  $^{26}\text{Al}/^{10}\text{Be}$

ratios to start with is likely small relative to the number of grains that have not undergone deep prior burial. Second, remobilizing deeply buried grains requires that they get exhumed to the surface, during which they will again accumulate cosmogenic nuclides that shift the ratios to higher values. For example, if our samples had been buried with a starting  $^{26}\text{Al}/^{10}\text{Be}$  ratio of ~7:1 to their current depth at a constant rate for 2 Myr, the  $^{26}\text{Al}/^{10}\text{Be}$  ratio would be ~2.7:1. If they would then exhume again at the same rate over the next 2 Myr, the  $^{26}\text{Al}/^{10}\text{Be}$  ratio would be ~5.3:1 when they reach the surface, yielding an apparent burial age of ~0.5 Ma. Third, although the upstream area of the Yarlung Tsangpo near the gorge is huge, the areas contributing material to the sediment transported by the river is most likely much smaller. By definition, depositional areas do not contribute any material. Eroding hillslopes contribute relatively more for increasing hillslope angles. Hence, it can be expected that the areas close to the sampling location, where hillslopes are steep (Fig. 2B), had been contributing relatively more material compared to the many flat areas farther upstream. Therefore, we think that recycled, previously buried material with  $^{26}\text{Al}/^{10}\text{Be}$  ratios lower than ~7:1 is not a significant source of uncertainty.

Because we don't exactly know the burial history, i.e., the time-depth history of our samples, we explored different burial scenarios (Figure S5, Figure S6). In all scenarios, we assume a wet bulk density of the sediment of  $2.1 \text{ g cm}^{-3}$ , which corresponds to sediment with a particle density of  $2.7 \text{ g cm}^{-3}$  and 35% saturated pore space. The first scenario serves for illustrative purposes and assumes instantaneous burial to depths where no more production of cosmogenic nuclides occurs ('A' in Figure S5, Figure S6A). In this case, the burial age lies between ~2 and 2.5 Ma and the corresponding cosmogenic nuclide-derived erosion rate is ~0.1-0.2 mm yr $^{-1}$ . In the second scenario we assume that burial occurred at a constant rate throughout the entire burial history ('B' in Figure S5, Figure S6B). This scenario is also rather unlikely, as we would assume that surface uplift rates and thus burial rates decreased with time as the Tsangpo Gorge was uplifted and river incision rates increased due to steepening of river gradients. Obviously, the additional production of cosmogenic nuclides during burial affects the total concentration of the sample. However, because most of the additional cosmogenic nuclide accumulation takes place in the upper few meters, that is, during the initial stages of the burial history, it mostly affects the inferred paleo-erosion rate but has only minor effect on the burial ages. The additional cosmogenic nuclide accumulation becomes important only for rather high paleo-erosion rates ( $>0.2 \text{ mm yr}^{-1}$ ), that is, when the inherited cosmogenic nuclide concentration is rather low. In the remaining two scenarios, we assumed burial rates that started out faster and slowed down with time ('C' and 'D' in Figure S5, Figure S6C and D). Both scenarios predict concentrations that lie in between the first two scenarios, but have only little effect on the burial ages of our samples. Thus, we conclude that for a range of burial scenarios, our samples yield consistent results, with burial ages of ~2-2.5 Ma and paleo-erosion rates of ~0.1-0.2 mm yr $^{-1}$ . Because our three samples stem from the same 3-m thick sand unit, we treat them as different estimates of the same depositional age and refer to the weighted mean concentration for our best estimate of the depositional age.

## **Supplementary Text**

### Author contributions

P. W. studied the cores and prepared the samples. D. S. conceived the study and together with J. L.-Z. led the development of this paper and the integration of the results. J. M. and D. S. conducted the ANN modelling. D. S. and J.-P. A. wrote the paper, with contribution from J. L.-Z. Y. Z. and D. Shi supervised the shallow drilling project and provided drill core material. All authors discussed the results and commented on the manuscript.

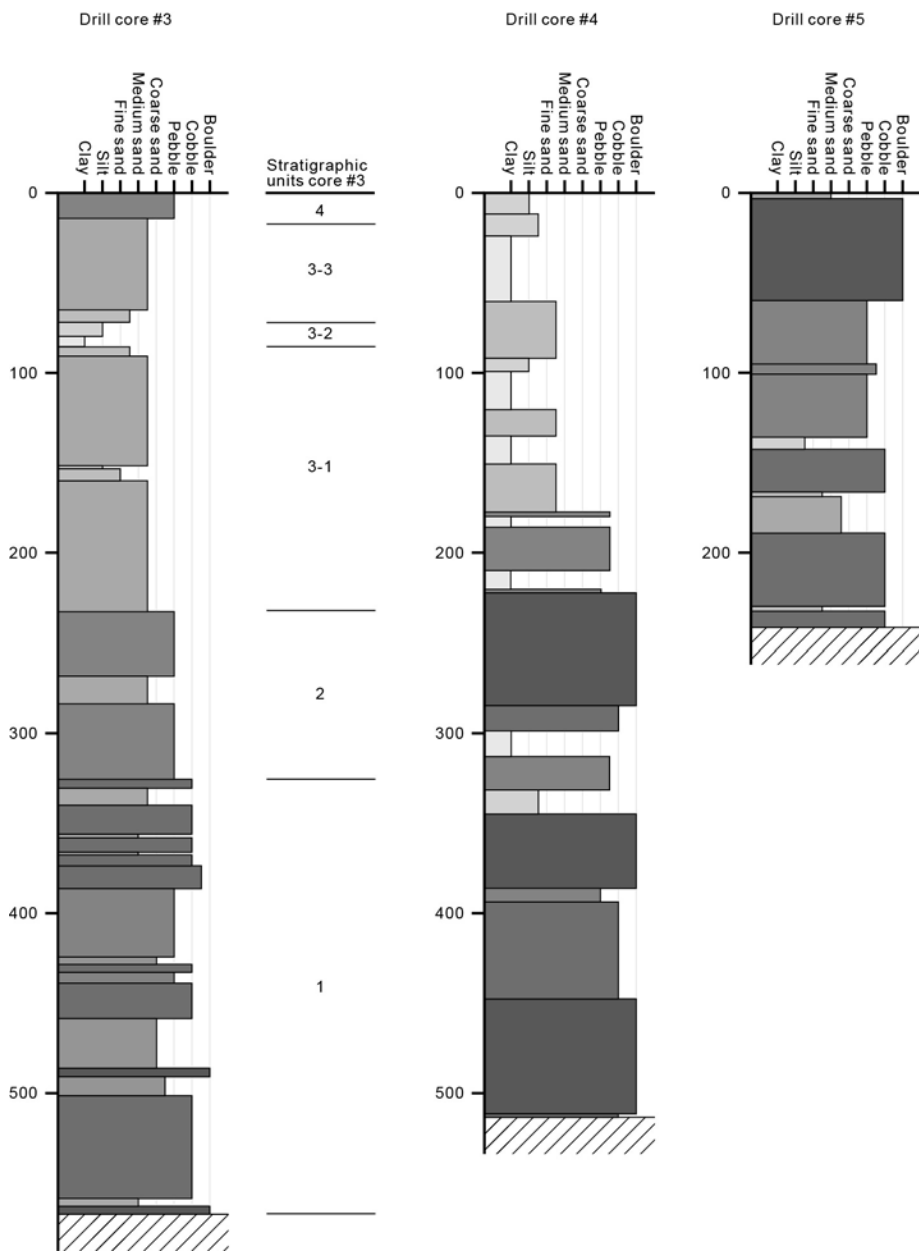


**Fig. S1.**

Simplified stratigraphic columns of the drill cores at sites #3-#5.



**Fig. S2**

Drill core recovered from drilling site #5 at a depth of 235.5-241.2 m. This section consists mainly of unconsolidated sand, gravel, and pebbles. Rounded pebbles near the bottom indicate fluvial transport. These deposits constitute the base of the valley fill at this site. The width of the box is ~1 m.



**Fig. S3**

Drill core recovered from drilling site #5 at a depth of 241.2-246.7 m. This section consists of gneissic bedrock. The width of the box is ~1 m.

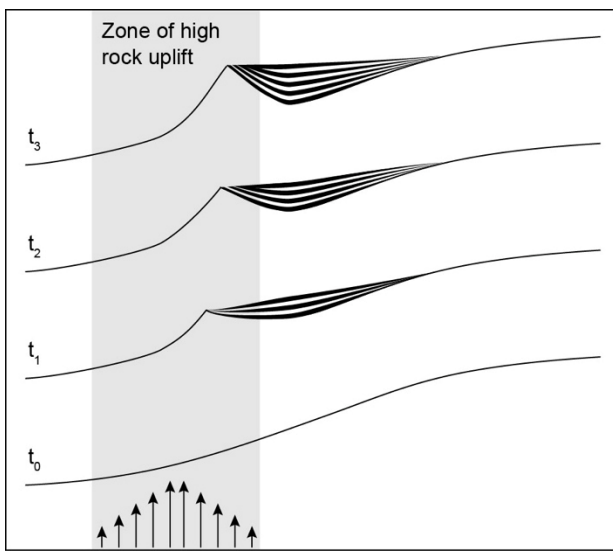


**Fig. S4**

Schematic illustration showing the response of a nearly graded river to localized uplift.  $t_0$  at bottom shows initial state, prior to uplift, and  $t_3$  at the top shows final state with steep river reach centred on zone of high rock uplift. During river steepening, sediments accumulated upstream of the zone of high rock uplift.

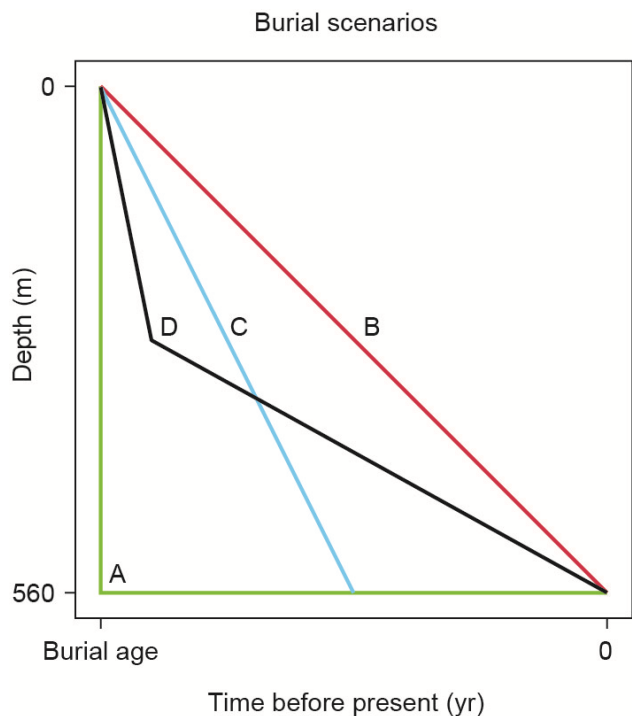


**Fig. S5**

Burial scenarios used for converting measured  $^{10}\text{Be}$  and  $^{26}\text{Al}$  concentrations to burial ages.

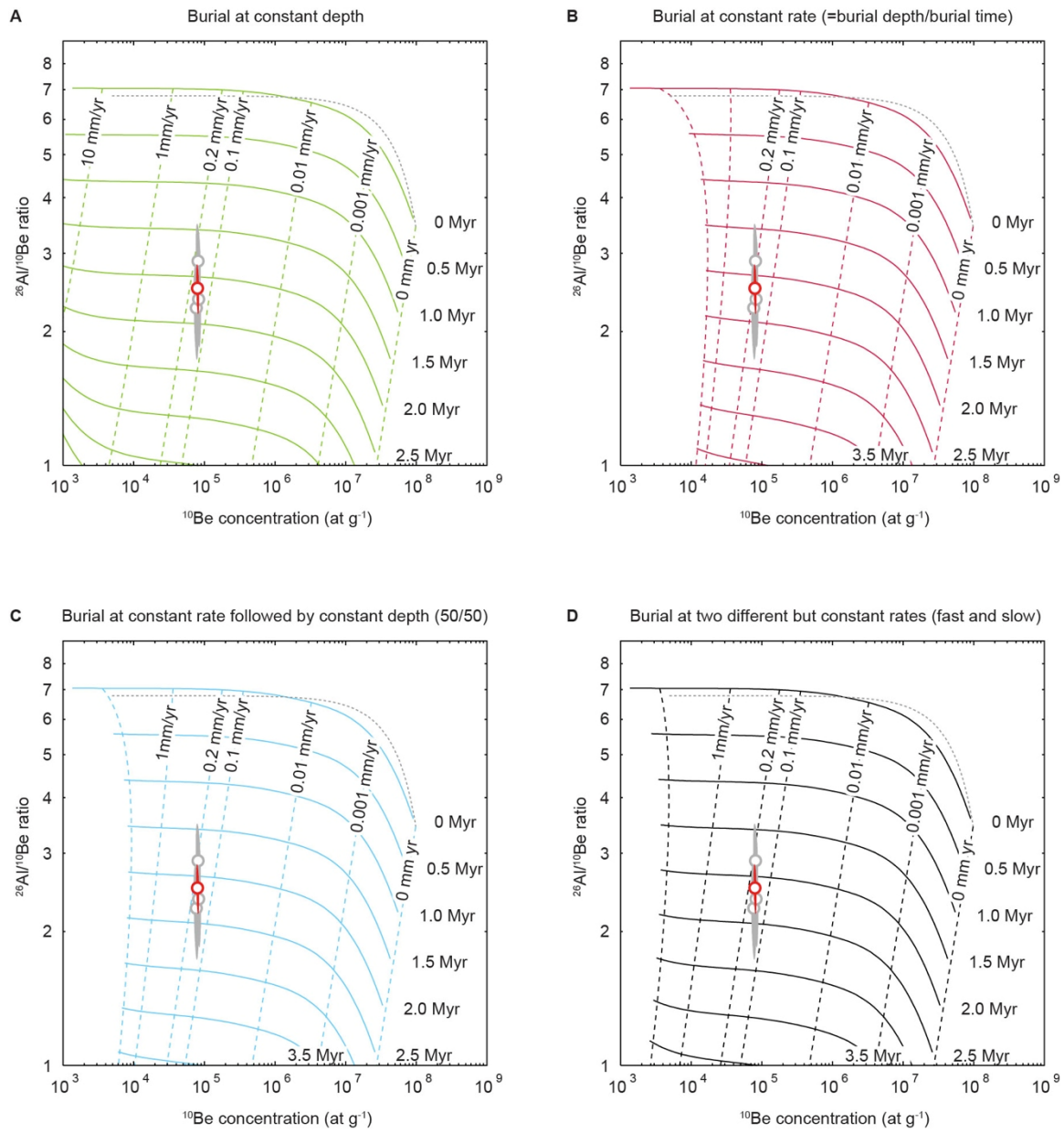


**Fig. S6**

Predicted combinations of burial age and paleo-erosion rate for the four burial scenarios shown in Fig. S4. Note that the concentrations correspond to the measured concentrations, that is, they have not been normalized by the site-specific scaling factors.

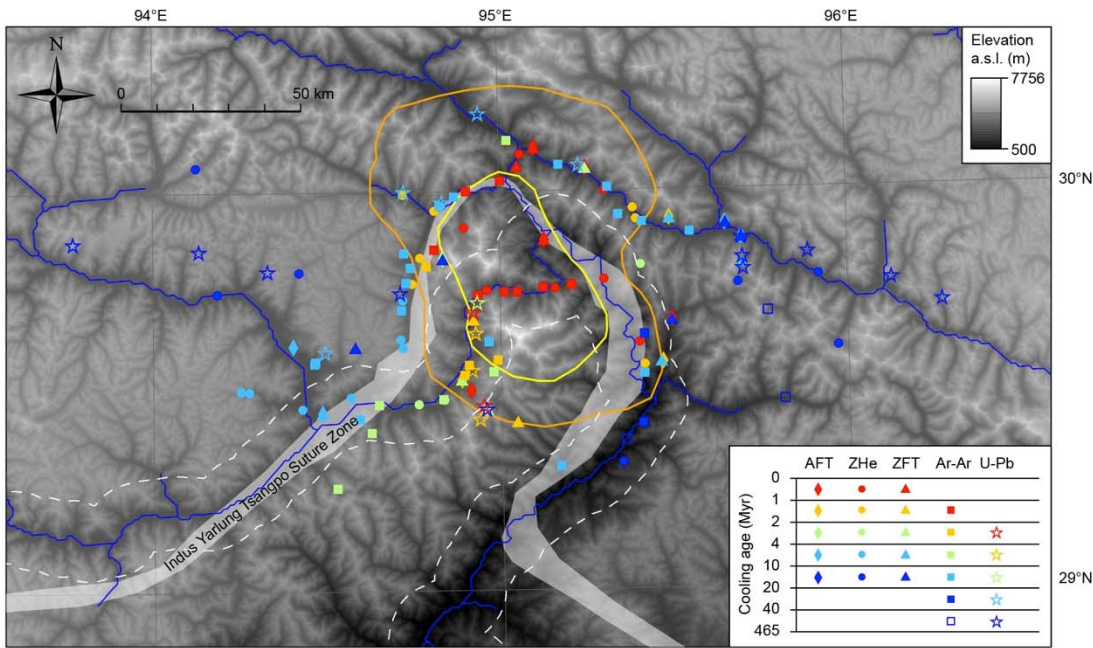


**Fig. S7**

Published bedrock cooling and crystallization ages. AFT = Apatite Fission Track (14,15); ZHe = Zircon U/Th-He (46); ZFT = Zircon Fission Track (14,15); Ar-Ar =  $^{40}\text{Ar}/^{39}\text{Ar}$  (47,48,49); U-Pb = Zircon Uranium-Lead (15,50). Contour lines show rapidly exhuming areas with young ( $<2$  Ma) Zircon U/Th-He (orange), and Biotite Ar-Ar ages (yellow) centered on the Tsangpo Gorge (18). Dashed white line extents 10-km to either side of Yarlung Tsangpo River and marks boundary for measuring hillslope angles shown in Fig. 2B and sampling cooling ages shown in Fig. 2C.

**Table S1.**

Description of stratigraphic units in the drill core from site #3.

Unit	Depth (m)	Description
4	0-20	Round to sub-rounded clast-supported pebble gravel in matrix of grayish yellow medium to coarse sand. Fluvial river bedload gravel
3-3	20-72	Grayish yellow pebbly medium to coarse sand.
3-2	72-85	Horizontal and thinly bedded layers of silty clay, with upward-fining and then coarsening sequence in grain size.
3-1	85-233	Gravely medium to coarse sand. Gravel consists mainly of 2-5 mm sub-angular small pebble of heterogeneous rock types, from gneiss, quartzite, sandstone to slate. Gray to grayish yellow.
2	233-325	Conglomerate of massive cobbley coarse pebbles in matrix of gray coarse-medium sand, interbedded with pebbly medium to coarse sand.
1	325-567	Alternating layers of pebbly gravel, cobbles to coarse pebbles, and pebbly sand and silt, interbedded with layers of well-sorted fine, medium sand. Weathering or soil formation in two layers of pebbly sandy silt. The basal 2m include cobbles to boulders, up to 200-400 mm size.
Bedrock	567-580	Bedrock. Moderately fractured and mildly weathered gneiss.

**Table S2.**

Analytical cosmogenic nuclide results.

Sample ID	Depth in drill core (m)	Sample mass dissolved (g)	$^{10}\text{Be}$ (atoms g $^{-1}$ )	$^{26}\text{Al}$ (atoms g $^{-1}$ )	$^{26}\text{Al}/^{10}\text{Be}$
WP1	561.7-561.9	64.84	$76630 \pm 2647$	$173108 \pm 16367$	$2.26 \pm 0.22$
WP2	562.5-562.7	61.55	$82012 \pm 2718$	$236525 \pm 18878$	$2.88 \pm 0.23$
WP3	563.5-563.8	73.16	$83706 \pm 2734$	$195646 \pm 17341$	$2.37 \pm 0.21$

**Table S3.**

Analytical ICP-OES results (ppm). Numbers directly below element symbols refer to wavelength (in nm).

Sample ID	Al 308.2	B 249.6	Ba 233.5	Ca 317.9	Cr 267.7	Fe 259.9	K 766.4	Li 670.7	Mg 279.0	Mn 257.6	Na 589.5	Ni 221.6
WP1	30.95	<0.01	0.16	18.43	0.44	<0.01	5.62	2.03	3.75	0.39	7.68	0.03
WP2	35.56	<0.01	0.16	17.81	0.05	9.19	5.60	2.00	3.80	0.36	7.24	<0.01
WP3	37.67	<0.01	0.23	18.56	0.08	12.05	8.17	2.79	3.59	0.55	9.35	0.03

## References

1. P. Tapponnier, X. Zhiqin, F. Roger, B. Meyer, N. Arnaud, G. Wittlinger, Y. Jingsui, Oblique stepwise rise and growth of the Tibet plateau. *Science* **294**, 1671–1677 (2001). [Medline](#) [doi:10.1126/science.105978](#)
2. E. R. Sobel, G. E. Hillel, M. R. Strecker, Formation of internally drained contractional basins by aridity-limited bedrock incision. *J. Geophys. Res.* **108** (B7), 2344 (2003). [doi:10.1029/2002JB001883](#)
3. J. Liu-Zeng, P. Tapponnier, Y. Gaudemer, L. Ding, Quantifying landscape differences across the Tibetan Plateau: Implications for topographic relief evolution. *J. Geophys. Res.* **113** (F4), F04018 (2008). [doi:10.1029/2007JF000897](#)
4. P. Molnar, W. R. Boos, D. S. Battisti, Orographic controls on climate and paleoclimate of Asia: Thermal and mechanical roles for the Tibetan Plateau. *Annu. Rev. Earth Planet. Sci.* **38**, 77–102 (2010). [doi:10.1146/annurev-earth-040809-152456](#)
5. M. K. Clark, L. M. Schoenbohm, L. H. Royden, K. X. Whipple, B. C. Burchfiel, X. Zhang, W. Tang, E. Wang, L. Chen, Surface uplift, tectonics, and erosion of eastern Tibet from large-scale drainage patterns. *Tectonics* **23**, n/a (2004). 10.1029/2002TC001402 [doi:10.1029/2002TC001402](#)
6. M. E. Brookfield, The evolution of the great river systems of southern Asia during the Cenozoic India-Asia collision: Rivers draining southwards. *Geomorphology* **22**, 285–312 (1998). [doi:10.1016/S0169-555X\(97\)00082-2](#)
7. P. Molnar, P. England, Late Cenozoic uplift of mountain ranges and global climate change: Chicken or egg? *Nature* **346**, 29–34 (1990). [doi:10.1038/346029a0](#)
8. J.-P. Avouac, E. B. Burov, Erosion as a driving mechanism of intracontinental mountain growth. *J. Geophys. Res.* **101** (B8), 17747–17769 (1996). [doi:10.1029/96JB01344](#)
9. P. Zeitler, A. S. Meltzer, P. O. Koons, D. Craw, B. Hallet, C. P. Chamberlain, W. S. F. Kidd, S. K. Park, L. Seeber, M. Bishop, J. Shroder, Erosion, Himalayan geodynamics, and the geomorphology of metamorphism. *GSA Today* **11**, 4–9 (2001). [doi:10.1130/1052-5173\(2001\)011<0004:EHGATG>2.0.CO;2](#)
10. P. O. Koons, P. K. Zeitler, B. Hallet, Tectonic Aneurysms and Mountain Building, in *Treatise on Geomorphology*, John F. Shroder, Ed. (Academic Press, San Diego 2013), pp. 318–349.
11. J. P. Burg, P. Nievergelt, F. Oberli, D. Seward, P. Davy, J.-C. Maurin, Z. Diao, M. Meier, The Namche Barwa syntaxis: Evidence for exhumation related to compressional crustal folding. *J. Asian Earth Sci.* **16**, 239–252 (1998). [doi:10.1016/S0743-9547\(98\)00002-6](#)
12. N. J. Finnegan, B. Hallet, D. R. Montgomery, P. K. Zeitler, J. O. Stone, A. M. Anders, L. Yuping, Coupling of rock uplift and river incision in the Namche Barwa-Gyala Peri massif, Tibet. *Geol. Soc. Am. Bull.* **120**, 142–155 (2008). [doi:10.1130/B26224.1](#)
13. D. Seward, J.-P. Burg, Growth of the Namche Barwa Syntaxis and associated evolution of the Tsangpo Gorge: Constraints from structural and thermochronological data. *Tectonophysics* **451**, 282–289 (2008). [doi:10.1016/j.tecto.2007.11.057](#)

14. D. W. Burbank, J. Leland, E. Fielding, R. S. Anderson, N. Brozovic, M. R. Reid, C. Duncan, Bedrock incision, rock uplift and threshold hillslopes in the northwestern Himalayas. *Nature* **379**, 505–510 (1996). [doi:10.1038/379505a0](https://doi.org/10.1038/379505a0)
15. J. L. Crowley, D. J. Waters, M. P. Searle, S. A. Bowring, Pleistocene melting and rapid exhumation of the Nanga Parbat massif, Pakistan: Age and P–T conditions of accessory mineral growth in migmatite and leucogranite. *Earth Planet. Sci. Lett.* **288**, 408–420 (2009). [doi:10.1016/j.epsl.2009.09.044](https://doi.org/10.1016/j.epsl.2009.09.044)
16. E. Enkelmann, T. A. Ehlers, P. K. Zeitler, B. Hallet, Denudation of the Namche Barwa antiform, eastern Himalaya. *Earth Planet. Sci. Lett.* **307**, 323–333 (2011). [doi:10.1016/j.epsl.2011.05.004](https://doi.org/10.1016/j.epsl.2011.05.004)
17. I. J. Larsen, D. R. Montgomery, Landslide erosion coupled to tectonics and river incision. *Nat. Geosci.* **5**, 468–473 (2012). [doi:10.1038/ngeo1479](https://doi.org/10.1038/ngeo1479)
18. L. Seeber, V. Gornitz, River profiles along the Himalayan arc as indicators of active tectonics. *Tectonophysics* **92**, 335–367 (1983). [doi:10.1016/0040-1951\(83\)90201-9](https://doi.org/10.1016/0040-1951(83)90201-9)
19. J. Lavé, J.-P. Avouac, Fluvial incision and tectonic uplift across the Himalayas of central Nepal. *J. Geophys. Res. Solid Earth* **106** (B11), 26561–26591 (2001). [doi:10.1029/2001JB000359](https://doi.org/10.1029/2001JB000359)
20. K. Hodges, J. M. Hurtado, K. X. Whipple, Southward extrusion of Tibetan crust and its effect on Himalayan tectonics. *Tectonics* **20**, 799–809 (2001). [doi:10.1029/2001TC001281](https://doi.org/10.1029/2001TC001281)
21. S. E. Cina, A. Yin, M. Grove, C. S. Dubey, D. P. Shukla, O. M. Lovera, T. K. Kelty, G. E. Gehrels, D. A. Foster, Gangdese arc detritus within the eastern Himalayan Neogene foreland basin: Implications for the Neogene evolution of the Yalu-Brahmaputra River system. *Earth Planet. Sci. Lett.* **285**, 150–162 (2009). [doi:10.1016/j.epsl.2009.06.005](https://doi.org/10.1016/j.epsl.2009.06.005)
22. F. Chirouze, P. Huyghe, P. van der Beek, C. Chauvel, T. Chakraborty, G. Dupont-Nivet, M. Bernet, Tectonics, exhumation, and drainage evolution of the eastern Himalaya since 13 Ma from detrital geochemistry and thermochronology, Kameng River Section, Arunachal Pradesh. *Geol. Soc. Am. Bull.* **125**, 523–538 (2013). [doi:10.1130/B30697.1](https://doi.org/10.1130/B30697.1)
23. K. A. Lang, K. W. Huntington, Antecedence of the Yarlung–Siang–Brahmaputra River, eastern Himalaya. *Earth Planet. Sci. Lett.* **397**, 145–158 (2014). [doi:10.1016/j.epsl.2014.04.026](https://doi.org/10.1016/j.epsl.2014.04.026)
24. D. R. Montgomery, B. Hallet, L. Yuping, N. Finnegan, A. Anders, A. Gillespie, H. M. Greenberg, Evidence for Holocene megafloods down the Tsangpo River Gorge, southeastern Tibet. *Quat. Res.* **62**, 201–207 (2004). [doi:10.1016/j.yqres.2004.06.008](https://doi.org/10.1016/j.yqres.2004.06.008)
25. O. Korup, D. R. Montgomery, Tibetan plateau river incision inhibited by glacial stabilization of the Tsangpo gorge. *Nature* **455**, 786–789 (2008). [Medline](#) [doi:10.1038/nature07322](https://doi.org/10.1038/nature07322)
26. Materials and methods are available in the supplementary materials on *Science Online*.
27. A. R. Duvall, M. K. Clark, B. Avdeev, K. A. Farley, Z. W. Chen, Widespread late Cenozoic increase in erosion rates across the interior of eastern Tibet constrained by detrital low-temperature thermochronometry. *Tectonics* **31**, TC3014 (2012). [doi:10.1029/2011TC002969](https://doi.org/10.1029/2011TC002969)

28. L. Seeber, A. Pecher, Strain partitioning along the Himalayan arc and the Nanga Parbat antiform. *Geology* **26**, 791–794 (1998). [doi:10.1130/0091-7613\(1998\)026<0791:SPATHA>2.3.CO;2](https://doi.org/10.1130/0091-7613(1998)026<0791:SPATHA>2.3.CO;2)
29. V. S. Cronin, W. P. Johnson, N. M. Johnson, G. D. Johnson, Chronostratigraphy of the upper Cenozoic Bunthang sequence and possible mechanisms controlling base level in Skardu intermontane basin, Karkakoram Himalaya, Pakistan, in *Tectonics of the Western Himalayas*, L. L. Malinconico, R. J. Lillie, Eds. (Geological Society of America, Boulder, CO, 1989), pp. 295–309.
30. Y. B. Seong, Absolute age determination of one of the oldest Quaternary(?) glacial deposit (Bunthang sequence) in the Tibetan Plateau using radioactive decay of cosmogenic  $^{10}\text{Be}$  and  $^{26}\text{Al}$ , the Central Karakoram, Pakistan: Implication for paleoenvironment and tectonics. *J. Korean Geogr. Soc.* **42**, 165–176 (2007).
31. G. K. C. Clarke, E. Berthier, C. G. Schoof, A. H. Jarosch, Neural networks applied to estimating subglacial topography and glacier volume. *J. Clim.* **22**, 2146–2160 (2009). [doi:10.1175/2008JCLI2572.1](https://doi.org/10.1175/2008JCLI2572.1)
32. C. P. Kohl, K. Nishiizumi, Chemical isolation of quartz for measurement of in-situ -produced cosmogenic nuclides. *Geochim. Cosmochim. Acta* **56**, 3583–3587 (1992). [doi:10.1016/0016-7037\(92\)90401-4](https://doi.org/10.1016/0016-7037(92)90401-4)
33. D. Lal, Cosmic-ray labeling of erosion surfaces: In situ nuclide production-rates and erosion models. *Earth Planet. Sci. Lett.* **104**, 424–439 (1991). [doi:10.1016/0012-821X\(91\)90220-C](https://doi.org/10.1016/0012-821X(91)90220-C)
34. J. C. Gosse, F. M. Phillips, Terrestrial in situ cosmogenic nuclides: Theory and applications. *Quat. Sci. Rev.* **20**, 1475–1560 (2001). [doi:10.1016/S0277-3791\(00\)00171-2](https://doi.org/10.1016/S0277-3791(00)00171-2)
35. D. E. Granger, J. W. Kirchner, R. Finkel, Spatially averaged long-term erosion rates from in-situ produced cosmogenic nuclides in alluvial sediment. *J. Geol.* **104**, 249–257 (1996). [doi:10.1086/629823](https://doi.org/10.1086/629823)
36. D. E. Granger, P. F. Muzikar, Dating sediment burial with in situ-produced cosmogenic nuclides: Theory, techniques, and limitations. *Earth Planet. Sci. Lett.* **188**, 269–281 (2001). [doi:10.1016/S0012-821X\(01\)00309-0](https://doi.org/10.1016/S0012-821X(01)00309-0)
37. J. Chmeleff, F. von Blanckenburg, K. Kossert, D. Jakob, Determination of the  $^{10}\text{Be}$  half-life by multicollector ICP-MS and liquid scintillation counting. *Nucl. Instr. Meth. Res. B* **268**, 192–199 (2010). [doi:10.1016/j.nimb.2009.09.012](https://doi.org/10.1016/j.nimb.2009.09.012)
38. G. Korschinek, A. Bergmaier, T. Faestermann, U. C. Gerstmann, K. Knie, G. Rugel, A. Wallner, I. Dillmann, G. Dollinger, C. L. von Gostomski, K. Kossert, M. Maiti, M. Poutivtsev, A. Remmert, A new value for the half-life of  $^{10}\text{Be}$  by heavy ion elastic recoil detection and liquid scintillation counting. *Nucl. Instr. Meth. Res. B* **268**, 187–191 (2010). [doi:10.1016/j.nimb.2009.09.020](https://doi.org/10.1016/j.nimb.2009.09.020)
39. T. L. Norris, A. J. Gancarz, D. J. Rokop, K. W. Thomas, Half-life of  $^{26}\text{Al}$ . *J. Geophys. Res.* **88** (S01), B331–B333 (1983). [doi:10.1029/JB088iS01p0B331](https://doi.org/10.1029/JB088iS01p0B331)

40. D. E. Granger, A. L. Smith, Dating buried sediments using radioactive decay and muogenic production of  $^{26}\text{Al}$  and  $^{10}\text{Be}$ . *Nucl. Instr. Meth. Res. B* **172**, 822–826 (2000). [doi:10.1016/S0168-583X\(00\)00087-2](https://doi.org/10.1016/S0168-583X(00)00087-2)
41. B. Heisinger, D. Lal, A. J. T. Jull, P. Kubik, S. Ivy-Ochs, S. Neumaier, K. Knie, V. Lazarev, E. Nolte, Production of selected cosmogenic radionuclides by muons: 1. Fast muons. *Earth Planet. Sci. Lett.* **200**, 345–355 (2002). [doi:10.1016/S0012-821X\(02\)00640-4](https://doi.org/10.1016/S0012-821X(02)00640-4)
42. B. Heisinger, D. Lal, A. J. T. Jull, P. Kubik, S. Ivy-Ochs, K. Knie, E. Nolte, Production of selected cosmogenic radionuclides by muons: 2. Capture of negative muons. *Earth Planet. Sci. Lett.* **200**, 357–369 (2002). [doi:10.1016/S0012-821X\(02\)00641-6](https://doi.org/10.1016/S0012-821X(02)00641-6)
43. G. Balco, J. Stone, N. Lifton, T. Dunai, A complete and easily accessible means of calculating surface exposure ages or erosion rates from  $^{10}\text{Be}$  and  $^{26}\text{Al}$  measurements. *Quat. Geochronol.* **3**, 174–195 (2008). [doi:10.1016/j.quageo.2007.12.001](https://doi.org/10.1016/j.quageo.2007.12.001)
44. D. E. Granger, C. S. Riebe, Cosmogenic nuclides in weathering and erosion, in J. I. Drever, Ed., *Surface and Ground Water, Weathering and Soils: Treatise on Geochemistry*, v. 5, 2nd ed. (Elsevier-Pergamon, Oxford, UK, 2007), chapter 14.
45. J. O. Stone, Air pressure and cosmogenic isotope production. *J. Geophys. Res.* **105** (B10), 23753–23759 (2000). [doi:10.1029/2000JB900181](https://doi.org/10.1029/2000JB900181)
46. M. Malloy, Rapid erosion at the Tsangpo knickpoint and exhumation of southeastern Tibet, M.S. thesis, Lehigh University, Bethlehem, PA (2004).
47. L. Ding, D. Zhong, A. Yin, P. Kapp, M. T. Harrison, Cenozoic structural and metamorphic evolution of the eastern Himalayan syntaxis (Namche Barwa). *Earth Planet. Sci. Lett.* **192**, 423–438 (2001). [doi:10.1016/S0012-821X\(01\)00463-0](https://doi.org/10.1016/S0012-821X(01)00463-0)
48. G. Quanru, P. Guitang, L. Zheng, Z. Chen, R. D. Fisher, Z. Sun, C. Ou, H. Dong, X. Wang, S. Li, X. Lou, H. Fu, The Eastern Himalayan syntaxis: Major tectonic domains, ophiolitic mélanges and geologic evolution. *J. Asian Earth Sci.* **27**, 265–285 (2006). [doi:10.1016/j.jseaes.2005.03.009](https://doi.org/10.1016/j.jseaes.2005.03.009)
49. P. K. Zeitler, M. A. Malloy, M. P. Kutney, B. D. Idleman, Y. Liu, W. S. F. Kidd, A. L. Booth, Geochronological evidence for the tectonic and topographic evolution of SE Tibet. *Eos* **87**, T23B-02 (2006). <http://adsabs.harvard.edu/abs/2006AGUFM.T32B..02Z>
50. A. L. Booth, P. K. Zeitler, W. S. F. Kidd, J. Wooden, Y. Liu, B. Idleman, M. Hren, C. P. Chamberlain, U-Pb zircon constraints on the tectonic evolution of southeastern Tibet, Namche Barwa area. *Am. J. Sci.* **304**, 889–929 (2004). [doi:10.2475/ajs.304.10.889](https://doi.org/10.2475/ajs.304.10.889)